HHS Public Access

Author manuscript

Brain Res. Author manuscript; available in PMC 2020 July 01.

Published in final edited form as:

Brain Res. 2019 July 01; 1714: 99–110. doi:10.1016/j.brainres.2019.02.027.

Sweet and bitter taste stimuli activate VTA projection neurons in the parabrachial nucleus

John D. Boughter Jr[1], **Lianyi Lu**[1], **Louis N. Saites**[1], **Kenichi Tokita**[2]

[1]Department of Anatomy & Neurobiology, University of Tennessee Health Science Center, Memphis, TN, 38163

[2]Institute of Natural Sciences, Senshu University, 3-8-1 Kanda-Jinbocho, Chiyoda-ku, Tokyo 101-8425, Japan

Abstract

This study investigated neural projections from the parabrachial nucleus (PBN), a gustatory and visceral processing area in the brainstem, to the ventral tegmental area (VTA) in the midbrain. The VTA contains a large population of dopaminergic neurons that have been shown to play a role in reward processing. Anterograde neural tracing methods were first used to confirm that a robust projection from the caudal PBN terminates in the dorsal VTA; this projection was larger on the contralateral side. In the next experiment, we combined dual retrograde tracing from the VTA and the gustatory ventral posteromedial thalamus (VPMpc) with taste-evoked Fos protein expression, which labels activated neurons. Mice were stimulated through an intraoral cannula with sucrose, quinine, or water, and PBN sections were processed for immunofluorescent detection of Fos and retrograde tracers. The distribution of tracer-labeled PBN neurons demonstrated that the populations of cells projecting to the VTA or VPMpc are largely independent. Quantification of cells double labeled for Fos and either tracer demonstrated that sucrose and quinine were equally effective in activating both pathways. These results indicate that information about both appetitive and aversive tastes is delivered to a key midbrain reward interface via direct projections from the PBN.

Keywords

Taste; Reward; Neuroanatomy; Tracer; Fos; Pathway

1. Introduction

At least five categories of primary taste quality exist: sweet, bitter, umami, sour, and salty (e.g. Chaudhari and Roper, 2010). Taste stimuli can also be classified according to hedonic value, i.e. whether they are appetitive or aversive (or somewhere in between). Furthermore,

Correspondence to be sent to: John Boughter Jr., Department of Anatomy & Neurobiology, University of Tennessee Health Science Center, Memphis, 38163, USA. jboughter@uthsc.edu.

some taste stimuli such as sugars are considered to be activators of reward: They are positively reinforcing, and their consumption elicits behavioral reactions indicative of pleasure or liking (Berridge and Kringelbach, 2008). The reinforcement aspect, which can also be described as “wanting”, is thought to be the purview of dopaminergic projections from the midbrain to the striatum (Berridge, 2007). In fact, sweet-tasting compounds evoke dopamine release in the ventral striatum, even in the absence of post-ingestive signals (Mark et al., 1991; Hajnal and Norgren, 2001; Hajnal et al., 2004; Tellez et al., 2016). How taste information engages canonical reward areas in the brain, however, is not completely understood (Yamamoto, 2006).

Taste information from peripheral receptors is relayed centrally through branches of three cranial nerves, which synapse in the rostral nucleus of the solitary tract (NST). In rodents, most of the gustatory projection neurons in the NST relay to caudal levels of the parabrachial nucleus of the pons (PBN) (e.g. Norgren, 1978; Monroe and Di Lorenzo, 1995; Karimnamazi et al., 2002). A number of taste-related projections arise from this nucleus, including to forebrain areas such as thalamus, hypothalamus, and amygdala (e.g. Norgren, 1974; Saper and Loewy, 1980; Voshart and Van Der Kooy, 1981; Fulwiler and Saper, 1984; Halsell, 1992; Tokita et al., 2010). Many of the forebrain areas that appear to utilize taste input, for example the central nucleus of amygdala (CeA) or lateral hypothalamus (LH), are also interconnected with reward areas such as the midbrain ventral tegmental area (VTA), and the nucleus accumbens (NAc), which is part of the ventral striatum in the forebrain (e.g. Cassell et al., 1999; Yamamoto, 2006; Beier et al., 2015; Nieh et al., 2015). Several studies support the presence of a direct connection from the PBN to the VTA (Phillipson, 1979; Coizet et al., 2010; Watabe-Uchida et al., 2012; Beier et al., 2015), although it is unknown if taste information is carried along this pathway.

In this study, we used neural tracing techniques to further investigate and characterize the PBN-VTA projection. We also used immunofluorescence to detect protein expression of the immediate early gene *c-fos* and investigate whether intraorally-administered taste stimuli in mice activate PBN neurons that project to the VTA. We compared this pathway to that of a better characterized taste projection: PBN neurons that project to the gustatory part of the thalamus, which is located in the most medial part of the ventral posteromedial thalamic nucleus (VPMpc). Previous studies show that VPMpc-projecting neurons are distributed throughout most regions of the PBN in mice (Hashimoto et al., 2009; Tokita et al., 2010). By quantifying the number of cells double-labeled for retrograde tracers and the Fos protein, we tested whether neurons responding to either specific taste qualities (and hedonic values) are preferentially represented in either PBN-VTA or PBN-VPMpc pathways.

2. Results

2.1. Anterograde Tracing of PBN efferents to the VTA and other targets

Injection sites for each mouse (section with maximum tracer deposit) varied in both size and location (Fig. 2). In a subset of mice, BDA injection sites were located either dorsal or ventral to the PBN, and in another mouse a small injection into the ventral end of the brachium conjunctivum did not appear to invade any PBN subnuclei. None of these off-target cases (n = 5) had axonal or terminal labeling in the VTA, VPMpc, or in any other

PBN projection fields defined in previous studies with rats (Norgren and Leonard, 1973; Saper and Loewy, 1980; Fulwiler and Saper, 1984; Krukoff et al., 1993; Karimnamazi and Travers, 1998) and mice (Hashimoto et al., 2009; Tokita et al., 2010). In the remaining cases, the injection sites were all located in the caudal PBN, centered either laterally (n=3) or medially (n= 5); two of the former cases had injection spread into the medial PBN as well. Notably, all cases produced a qualitatively similar pattern of labeling in mid- and forebrain regions. However, while labeling was very robust in the two mice with more encompassing, laterally-centered injections, it was sparser in the other cases. Staining for BDA in various brain regions appeared as either punctate varicosities, representative of terminal-like arborizations, or linear profiles, indicative of axonal labeling.

Overall, PBN projections were found to be bilateral, with the label generally more robust on the ipsilateral side (but see below). Labeling was seen in the contralateral PBN (Fig. 2C), in the lateral and ventral periaqueductal gray, midbrain reticular nucleus, VTA, and substantia nigra pars compacta (SNc) (Fig. 2F–H). In the forebrain, label was present in both the thalamus (chiefly VPMpc, parafascicular, and central medial divisions; Fig. 2D) and hypothalamus (including lateral, paraventricular and dorsomedial divisions; Fig. 2E). Labeling was also present in the central and basomedial amygdala (Fig. 2E), and bed nucleus of the stria terminalis. In some mice, light terminal label was also found in the insular cortex, including in the granular and dysgranular divisions (i.e. gustatory cortex).

In the 2 mice with PBN injection sites that included both medial and lateral regions, labeling in the VTA began at its caudal border (about – 3.6 relative to bregma) and persisted through its rostral-caudal extent. Labeling was found in the dorsal portion (both medial and lateral) of the parabrachial pigmented nucleus (PBP) subdivision of the VTA; it was not evident in midline subdivisions. VTA label was exceptional in that it was always found to be more robust on the contralateral side, as opposed to labeling in the SNc, which was stronger ipsilaterally. To better define the nature of this projection to the midbrain, we examined the brains of two mice where fluorescent microruby was used as the anterograde tracer; in both cases, midbrain sections were counterstained for tyrosine hydroxylase (TH) to delineate the large field of dopaminergic neurons found in the VTA (i.e., cell group A10). Consistent with the BDA cases, labeled axons and terminals were strongest in the dorsal part of the PBP, and were also found along the SNc (Fig. 3). A higher magnification view revealed overlap of labeled terminals and what appeared to be dendritic processes of TH+ cells, suggesting (but not proving) synaptic contacts between PBN afferents and dopaminergic (DA) cells. As microruby can also (to some extent) be transported retrogradely, a handful of filled (but not double-labeled) cell bodies were also found in the VTA, suggestive of descending, reciprocal projections from this region to the PBN (Tokita et al., 2009).

2.2 Retrograde tracing of PBN projections to the VTA and VPMpc

Injections sites for the retrograde tracers Fluorogold (FG) and cholera toxin b (CTb) in the VTA and VPMpc, respectively, were reconstructed for all mice (Fig. 4). The overall size and accuracy (estimated amount of tracer within the delineated target region) was not significantly correlated with the number of either type of tracer-labeled cell in the PBN. Retrograde neuronal labeling with either FG (VTA-projecting cells) or CTb (VPMpc-

projecting cells) was found throughout the PBN, but in distinct patterns for each projection (Fig. 4C–F). Consistent with the anterograde tracing results, VTA-projecting cells were always found in greater numbers on the contralateral side and tended to be located dorsally within the PBN. On the other hand, VPMpc-projecting cells were more numerous ipsilaterally. These were found distributed widely in both medial and lateral subnuclei, including within the el subnucleus. Both types of labeled cells were found in the gustatory "waist" region, i.e. the medial (m), ventral lateral (vl) and bc subnuclei. At a basic level of analysis, we counted roughly equal numbers of total labeled cells per mouse (n = 14) labeled with either FG (mean = 706.5) or CTb (mean = 780.6; paired *t* not significant). However, there was greater variability among individual mice for CTb labeling (48.9% coefficient of variation, or CV) as compared to FG (29.6% CV). Total cell counts for each tracer were not correlated among mice (Pearson $r = 0.13$, $p = 0.66$).

As the distribution of retrogradely-labeled cells for either tracer was not affected by intraoral stimulus group, data were combined across group for quantitative analysis of subnuclear expression (see methods). Tracer expression according to side and subnucleus, and rostral-caudal (R-C) level, is displayed in Fig. 5. Overall, more FG (VTA-projecting) cells were found on the contralateral side (mean cell counts = 284.86 vs. 421.64 for ipsilateral and contralateral sides, respectively). A 2-way repeated measures ANOVA (side X subnucleus) indicated significant main effects of side ($F_{[1,14]} = 39.82$, $p < 0.001$) and subnucleus ($F_{[8,104]} = 74.84$, $p < 0.001$), as well as a significant interaction ($F_{[8,104]} = 13.56$, $p < 0.001$). Mean cell counts for each subnucleus ranged from 2.29 – 102.7 contralaterally, and 3.5 – 82.21 ipsilaterally. FG cells were found in highest numbers within dorsal medial (dm), m, vl, and central lateral (cl) subnuclei, especially on the contralateral side, and at caudal levels for the medially-located subnuclei (Fig. 5A,B).

Unlike FG, CTb was expressed in overall greater numbers on the ipsilateral side (mean counts = 578.36 vs. 202.21 for ipsilateral and contralateral sides, respectively). CTb also varied from FG in its subnuclear expression, notably in its weak expression in the dm and robust expression in the external lateral (el) subnucleus. Results of a two-way repeated measures ANOVA (side X subnucleus) indicated significant main effects of side ($F_{[1,14]} = 89.49$, $p < 0.001$) and subnucleus ($F_{[8,104]} = 117.96$, $p < 0.001$), and a significant interaction ($F_{[8,104]} = 45.64$, $p < 0.001$). Mean cell counts for each subnucleus ranged from 8.5 – 132.1 ipsilaterally, and 2.93 – 64.21 contralaterally. CTb expression was significantly elevated on the ipsilateral side in the m, bc, cl, and el subnuclei (Fig. 5C,D). Finally, we also quantified the number of cells that appeared to be doubled-labeled for both tracer. Only a handful of cells were found to collateralize to both VTA and VPMpc (3–7 per mouse, either side); this result, in addition to the distinct subnuclear expression of either tracer, reflects the independence of these projections.

2.3 Quantification of Fos-IR and double-labeled cells

As in previous studies, different intraoral stimuli produced distinct patterns of activity in the PBN. Examples of Fos-immunoreactive (Fos-IR) cells, and of cells double-labeled (DL) for Fos and tracer, in various regions of the PBN are shown in Fig. 6. Total counts of Fos-IR PBN cells among mice (combined across side and subnucleus) varied according to stimulus,

with stronger expression in mice given intraoral sucrose (mean number of cells = 685.17 ± 51.04) or quinine (602 ± 125.45) relative to water (154 ± 42.17). Cell counts were averaged across side (see methods) to investigate the possible relationship between stimulus and subnucleus. A 2-way mixed ANOVA (stimulus X subnucleus) yielded significant main effects of both stimulus ($F_{[2,11]} = 13.82$, $p < 0.001$) and subnucleus ($F_{[8,88]} = 23.83$, $p < 0.001$), as well as a significant interaction ($F_{[16,88]} = 6.33$, $p < 0.001$). Post-hoc multiple comparison tests between stimuli indicated significant differences in 5/9 subnuclei (Fig. 7A). Each stimulus evoked different numbers of Fos-IR cells in the dm, with QHCl the most effective stimulus, and water the least. Sucrose and QHCl stimulation resulted in more Fos-IR cells than did water in the m and el, whereas sucrose was the most effective stimulus in the cl and dl. Sucrose was a particularly effective stimulus in the m subnucleus at caudal levels compared to quinine (Fig. 7B) or water, while the strongest Fos expression evoked by QHCl was found rostrally.

Overall, there were about twice as many CTb-Fos DL cells found per mouse as there were FG-Fos DL cells (mean = 49.29 ± 11.18 for CTb and 24.0 ± 5.76 for FG; paired $t = 2.17$, $p = 0.049$). Generally, more FG-Fos DL cells were found on either side of the brain in the dm, m, vl and cl than in other subnuclei, reflecting the distribution of FG cells themselves. As other subnuclei contained little double labeling, FG-Fos DL cells were summed across subnuclei in either the medial or lateral PBN and examined as a percentage of the total amount of tracer-expressing cells on either side of the brain (i.e., in 4 “regions”; Fig. 7C). This DL/tracer ratio reveals how effective a stimulus was in activating a population of projection neurons and assumes that the number of tracer-expressing cells did not vary meaningfully among stimulus groups, which was the case here. A 2-way mixed ANOVA (region X stimulus) yielded main effects of both region ($F_{[3,33]} = 5.52$, $p = 0.011$) and stimulus ($F_{[2,11]} = 5.87$, $p = 0.018$), but the interaction was not significant. Posthoc tests (collapsed across region) indicated that sucrose activated significantly more VTA-projection cells than water, with the order of effectiveness sucrose > QHCl > water. CTb-Fos DL cells were found in greatest amounts ipsilaterally, including in the m, bc, vl and el subnuclei. A 2-way mixed ANOVA indicated significant effects of region ($F_{[3,33]} = 7.85$, $p = 0.002$) and stimulus ($F_{[2,11]} = 9.34$, $p = 0.004$), as well as a significant interaction ($F_{[6,33]} = 3.17$, $p = 0.031$). Posthoc tests showed that QHCl and sucrose activated more VPMpc-projecting cells than water, especially in the ipsilateral lateral subnuclei (Fig. 7E).

The number of DL cells may also be influenced by the number of available Fos-IR cells resulting from stimulation with a particular tastant. When DL/Fos ratios were examined for each type of DL cell in each region, there were no significant differences according to stimulus. Mean DL/tracer and DL/Fos ratios (based on overall counts per animal) for each cell type and stimulus are compared in Fig. 7D and7F. The percentage of DL cells evoked by water increases relative to the other stimuli when expressed as a percentage of total Fos-IR cells. In other words, despite much lower levels of water-evoked Fos-IR in the PBN, the proportion of projection cells that is activated is not different from the 2 taste stimuli.

3. Discussion

3.1 Summary of Results

There is evidence that neurons in the PBN project directly to the VTA (e.g. Coizet et al., 2010; Beier et al., 2015). However, it is unclear whether or not PBN neurons that function in taste or intraoral sensation are part of this direct pathway. We first used anterograde tracing techniques to show that the PBN to VTA projection was stronger on the contralateral side, and that many PBN cells appear to make direct contact with dopaminergic neurons in the VTA. Using a combination of retrograde tracing and taste stimulus-evoked Fos, we show that the PBN neurons that project to VTA are a population distinct from those that project to the gustatory thalamic relay. Sucrose tended to activate more VTA-projecting neurons than either quinine or water, although this effectiveness was dependent on which PBN region was examined.

3.2. Technical considerations

Although Fos immunoreactivity is a useful technique for visualization of neuronal activity in a spatially informative manner throughout the brains of animals, it has several aspects that should be considered: The relative strength of a response is not particularly evident in single neurons, physiological activity and Fos expression are not always correlated (Fenelon et al., 1993), and some brain areas show constitutive expression of Fos protein, making discrimination of actual stimulus-evoked activity problematic (e.g. Kovacs, 2008). Furthermore, the strength of Fos expression in sensory cortices (including gustatory cortex) depends on the experience of the animal (Bamji-Stocke et al., 2018).

Administration of intraoral taste stimuli generally cause an increase in number of Fos-IR cells (relative to controls) in brain areas with known gustatory function. At least some amount of this expression is dependent on peripheral taste input (Yamamoto et al., 1993; King et al., 2003; Tokita et al., 2007; Riley and King, 2013). Moreover, stimuli of different qualities evoke distinct spatial patterns (Yamamoto et al., 1994; Tokita et al., 2014), and for some stimuli (such as NaCl) there is at least rough concordance between Fos pattern and the distribution of taste-responsive cells as measured by electrophysiology (Ogawa et al., 1987; Yamamoto et al., 1994). Here, we examined Fos in the PBN in cells labeled with retrograde tracers (FG and CTb). FG expression has shown in at least one study to interfere with (reduce) Fos expression (Franklin and Druhan, 2000), although in our study we did not see significant variation in counts of Fos-IR cells according to brain side, despite robust side differences in tracer expression.

Another issue is the nature of stimulation through the IO cannula, and its relationship to taste and ingestion. Although we chose concentrations of two novel stimuli that are capable of evoking salient orosensory-based behavioral responses in B6 mice (Boughter et al., 2005; Dotson and Spector, 2007), they are likely also evoking responses in non-gustatory pathways. Mice are surely consuming sucrose, and possibly water, throughout the 20-minute test session; hence these stimuli are associated with postingestive (visceral) activity. It is even possible that some quinine is ingested, although the behavior of the mice suggested active rejection of this stimulus (data not shown). In a previous study, Yamamoto and Sawa

(2000) compared IO-delivered stimuli to direct gastric stimulation in rats. In the PBN, quinine and saccharine both evoked substantially more Fos when delivered intraorally, especially at caudal levels. IO sucrose also resulted in a substantial increase in number of Fos-IR cells relative to intragastric delivery, although this disparity diminishes rostrally and finally reverses at the most rostral level examined. We only counted cells in the more caudal part of the PBN, although this does not obviate the possibility that a portion of our IO-evoked Fos is postingestive, rather than orosensory, in nature. Finally, it is also possible that activation of some PBN neurons during stimulation is related to tactile stimulation, nociception, arousal, hunger, thirst, or some other process.

Overall, a modest amount of DL cells were found in this study relative to numbers of tracer-labeled or Fos-IR cells. Considering all individual PBN subnuclei and stimulus groups, DL/tracer ratios ranged from 0 to about 20% (for both tracers), with averaged values for the tastants closer to 5–10% (i.e., Figure 7). However, it is worth pointing out that the percentages reported here are in line with those from other studies examining tracer (FG or CTb) and Fos co-expression (Travers and Hu, 2000; Kang et al., 2011; Tokita et al., 2014; Yokota et al., 2015; Jin and Maren, 2015). Furthermore, it is also likely that the true number of taste-activated projection neurons can only be accurately estimated by adding together numbers of double-labeled cells resulting from stimulation with each individual taste quality.

3.3. Neuroanatomy of the PBN-to-VTA projection

Both anterograde and retrograde tracing confirmed the existence of a robust, bilateral population of PBN neurons that project to the VTA in the midbrain. The existence of this pontine-midbrain pathway (including PBN efferents to the neighboring SNc) in rodents has been noted in previous studies (Phillipson, 1979; Saper and Loewy, 1980; Coizet et al., 2010; Watabe-Uchida et al., 2012; Beier et al., 2015). Axons from both medial and lateral PBN travel dorsally and anteriorly as part of the central tegmental tract to enter the SNc and then the VTA; some of these fibers cross the midline (Saper and Lowey, 1980; Coizet et al., 2010). Here we show that the VTA receives a proportionally larger input from the contralateral PBN. This asymmetry appears to be consistent with the projections described in rats by Saper and Loewy (1990), although it's not explicitly discussed in their report. PBN terminals were found distributed in the dorsal part of the PBN, predominantly in the PBP subnucleus, including close approximation of some (but not all) terminals with densely packed TH^+ cell bodies and dendrites as described previously in rats (Coizet et al., 2010). Using viral-genetic tracing techniques in mice, Beier et al. (2015) showed that both VTA DA and GABAergic neurons receive PBN inputs; these particular DA cells project to NAc, medial prefrontal cortex, or the amygdala. The relationship of specific VTA subnuclei, including the PBP, to specific aspects of reward is not entirely clear (Sanchez-Catalan et al., 2014). The most salient relationships between neuroanatomical position within the VTA and function appear to involve variation between anterior and posterior (Sanchez-Catalan et al., 2014), or medial and lateral (e.g. Beier et al., 2015) location. In the present study, however, PBN terminal/axonal labeling was found distributed across both of these axes.

Following retrograde tracing, VTA-projecting cells were found on either side of the brain distributed in both medial and lateral subnuclei, and throughout the rostral-caudal extent of

the portion of the PBN investigated here. This includes cells distributed in the caudal gustatory waist region (i.e. m, vl, and bc), which has been shown in mice to contain the largest concentration of taste-responsive neurons (Tokita et al., 2016). Interestingly, however, the distribution of VTA-projecting neurons within the PBN was found to be distinct from that of cells projecting to the VPMpc. Both populate the waist area, although few cells double-labeled with both tracers were found. Also, few VTA-projecting cells were found in the el, a subnucleus shown previously to respond to aversive taste, visceral, and oral nociceptive stimuli (e.g. Yamamoto et al., 1994; Hashimoto et al., 2009; Li and Lemon, 2019). A large population of neurons expressing calcitonin gene-related peptide (CGRP) is located in the el (e.g. Carter et al., 2013). These neurons have been shown to respond to a variety of noxious sensory stimuli, including stimuli associated with pain, fear, and satiety (Campos et al., 2018), leading Palmiter (2018) to conclude that they play a key role in the rodent CNS as general danger or threat detectors.

3.4. Gustatory function of the PBN-VTA pathway

It has long been appreciated that consumption of sweet-tasting compounds is associated with reward, i.e. these stimuli are positively reinforcing and elicit positive hedonic reactions (Berridge and Robinson, 1998; Redgrave et al., 1999). Consumption of sugars and sweeteners produces an efflux of dopamine in the NAc of rodents, even in the absence of post-oral signals or calories (Mark et al., 1991; Hajnal and Norgren, 2001; Hajnal et al., 2004; Tellez et al., 2016). In rats, this taste-elicited response was dependent on an intact PBN, but unaffected by lesions of the VPMpc (Hajnal and Norgren, 2005). How taste information gets from the PBN to the NAc to modulate DA release, however, has been unclear. The existence of taste-responsive VTA-projecting PBN neurons suggests that these neurons may directly modulate the activity of DA cells in the VTA, which project to the NAc. Lesions of the VTA result in a reduction of sucrose preference in both rats (Shimura et al., 2002; Shibata et al., 2009) and mice (Martinez-Hernandez et al., 2006). Whether a taste-specific neural signature can be localized in the VTA, though, is not clear. There is considerable complexity and diversity in how midbrain DA neurons respond to rewarding or reward-related stimuli, including sweet-tasting food stimuli, in physiological studies (e.g. Shultz et al., 1997; Ungless, 2004; Takahashi et al., 2017). Fos expression in the VTA evoked by palatable foods or sweet stimuli may be dependent on factors such as learning or experience (e.g. Mungardee et al., 2008; Park and Carr, 1998; Dela Cruz et al., 2016; Figlewicz et al., 2011).

In this study we also found that an intensely bitter stimulus, 0.003 M quinine, activated VTA-projecting PBN neurons in some regions almost as effectively as sucrose. This is perhaps not surprising, given that other types of aversive stimuli have been shown to activate a subset of DA neurons in VTA, including footshock (Brishoux et al., 2009). Other DA neurons in VTA are inhibited by aversive stimuli, likely through local inhibition following activation of GABA neurons (e.g., Tan et al., 2012). Inhibition of the PBN leads to a reduction of firing rate of DA neurons, and a suppression of the phasic inhibitory response to footshock (Coizet et al., 2010). Evidence for quinine-evoked DA release in the forebrain (prefrontal cortex and striatum) is equivocal (Bassareo et al., 2002; Tellez et al., 2016). Both

hedonic “hot spots” and “cold spots” are found in the NAc, although dopamine release itself does not regulate pleasure (Berridge, 2007; Berridge and Kringelbach, 2015).

Aside from the PBN-VTA projection, there are other possible routes by which a taste signal may modulate DA release in the striatum. Taste-responsive cells in the NST and PBN project to forebrain areas such as the CeA and LH, both of which are interconnected with the VTA and NAc (Yamamoto, 2006). There is also some electrophysiological evidence that PBN taste neurons project directly to the NAc (Li et al., 2012), although anatomical experiments suggest this is at best a sparse projection (Saper and Loewy, 1980; Brog et al., 1993; Mungarndee et al., 2008). In our preliminary studies, we placed FG or CTb in the NAc of a few mice and saw relatively small amounts of labeled neurons scattered in the ventral-medial PBN, but not in the gustatory waist area (data not shown).

3.5 Post-ingestive function of the PBN-VTA pathway

The PBN plays an important role in post-ingestive processing and satiety (Zseli et al., 2016; Palmiter, 2018), and this nucleus has been implicated in peptidergic suppression of VTA-dependent DA release (which leads to inhibition of eating; Whiting et al., 2017). Direct input from the caudal, visceral NST is found throughout the PBN but is densest at rostral levels, especially in lateral subnuclei (Karimnamazi et al., 2002). $CGRP^+$ PBN neurons receive input from hypothalamic neurons expressing agouti-related protein (AgRP), and activation of $CGRP^+$ neurons inhibits feeding even in hungry mice (Carter et al., 2013). These neurons are primarily clustered in the el, and project to the CeA and bed nucleus of the stria terminalis (D’Hanis et al., 2007; Palmiter, 2018). However, we did not find many VTA-projection neurons in this region, suggesting that if a PBN-VTA signal plays a role in satiety, it likely does so through indirect connections. Tellez et al. (2016) posit that while reward-related information about sweetness (taste) reaches the NAc via the VTA, information about calories is communicated to the dorsal striatum via the SNc. Additional studies are necessary to more carefully distinguish and delineate the relative role of PBN-VTA projection neurons in taste and feeding, and how their activity is related to reward processing.

3.6 The PBN-VPMpc projection

VPMpc-projecting neurons were located in almost all PBN subnuclei, with the largest numbers being located in the ipsilateral m and el subnuclei. This pattern is very similar to our previous mouse study using a different retrograde tracer (Tokita et al., 2010), and is consistent with other studies in rodents (e.g. Voshart and Van Der Kooy; Fulwiler and Saper, 1984; Halsell, 1992; Hashimoto et al., 2009). As mentioned above, the el is an area with strong visceral representation/function. Hashimoto et al. (2009) suggested that the inner part of the el in mice conveys both taste and viscerosensory signals, whereas the outer part of this subnucleus conveys only viscerosensory signals, based on their results that VPM-projecting cells were predominantly found in the inner part of the el. In our study, a higher percentage of VPMpc-projecting neurons were activated by either sucrose or quinine than by water, especially in lateral subnuclei ipsilaterally. The thalamocortical taste pathway has been conceptualized by some to be a pathway primarily involved in coding sensory aspects of taste stimuli, as opposed to limbic or midbrain projections, which favor taste-related

learning, appetitive behavior, or reward-related processing (Yamamoto et al., 1994; Sewards, 2004; Yamamoto, 2006; Smith and Boughter, 2009). In this schema the VPMpc is often characterized as a simple “relay” to the cortex. This notion is of course oversimplified, and there is recent evidence that the gustatory thalamus plays important, functional roles in coding both stimulus identity and palatability, as well as expectation (e.g., Liu and Fontanini, 2015).

4. Experimental procedure

4.1. Animals

Adult male and female C57BL6/6J (B6) mice (20 – 38 g) were used in all experiments. This included 19 mice for anterograde tracing experiments and 23 mice for the retrograde tracing experiment; a subset of these were included in the final analysis for either approach (15 and 14, respectively) based on successful tracer injections. All animals were maintained in a temperature- and humidity-controlled colony room on a 12 h light/12 h dark cycle (lights on at 0700 h, off at 1900 h), and were given access to normal dry pellet (Teklad 7912, Harlan Teklad, Madison, WI, USA) and water. Food and water were available *ad libitum* except on the testing day and part of the previous day (see below). This study was approved by the Animal Care and Use Committee at UTHSC, and all experiments were carried out in accordance with the National Institute of Health Guide for Care and Use of Laboratory Animals (8^{th} edition, 2011).

For anterograde tracing, 14 mice (6 females, 9 males) received unilateral injections of biotinylated dextran amine (BDA), and 5 mice (4 females, 1 male) unilateral injections of microruby (a fluorescent dextran) into the PBN. In the former group, one mouse was used as a control for BDA immunohistochemistry (no injection was made, and no labeling was seen), and size and location of injection sites in the remaining mice were related to terminal distribution. 2 mice injected with microruby were selected for further immunocytochemistry and microscopic analysis based on injection site. For dual retrograde tracing combined with immunoflourescent detection of Fos protein expression, data were analyzed from a total of 14 mice (10 male, 4 female) with successful injections of both tracers, divided into 3 groups based on intraoral stimulus (Ns = 6 sucrose, 4, QHCl, 4 water). Nine additional mice were excluded from this experiment due to unsuccessful tracer injections (i.e., one or the other injection not expelled properly, or not on target).

4.2 Surgical injection of tracers and implantation of intraoral cannulas.

Prior to tracer injection, mice were anesthetized with intraperitoneal injection of ketamine/xylazine (100/10 mg/kg) and positioned in a stereotaxic frame. The scalp was opened with a midline incision, and the skull was leveled between bregma and lambda by adjusting the bite bar. Body temperature was maintained at 35 °C using a heating pad. Neuronal tracers were injected from a glass micropipette (30–35 μm tip diameter) driven by a micromanipulator (SM-191, Narishige, Tokyo, Japan). For anterograde tracing, unilateral injections (either iontophoresis or pressure injection) of either 10% BDA (10,000 MW, Invitrogen Corporation, Carlsbad, CA, USA) or 10% microruby dextran (3000 MW, Invitrogen Corporation, Carlsbad, CA, USA) were made into the PBN (right side; 5.34 mm posterior,

1.2 mm lateral, 3.4 mm ventral with respect to bregma). For retrograde tracing, 5% Fluorogold (FG; Fluorochrome, LLC, Denver, CO, USA) was iontophoretically injected (2 μA, 8 s on/off for 20 min) into the right VTA (3.1 anterior, 0.5 lateral, 4.4 mm ventral to bregma), and 1 μl of 0.2% Cholera toxin subunit b (CTb; List Biological Labs, Campbell, CA, USA) was pressure injected into the right VPMpc (1.9 mm anterior, 0.6 mm lateral, 4.2 mm ventral relative to bregma). The position of the injection pipette was not altered 10 min prior to and 10 min following tracer injection.

In the retrograde groups, following injection of both tracers, polyethylene tubing (PE 50) was inserted (with the aid of a 25 g needle) through the right buccal mucosa and led along the lateral surface of the skull. The needle was removed, and the resulting cannula was secured to the skull using dental acrylic and screws. The oral end of the cannula was placed between the cheek and gum next to the first maxillary molar and flattened by flaring to prevent it from being drawn into the oral mucosa. These intraoral cannulas were inserted unilaterally, ipsilateral to the tracer injection.

4.3 Intraoral stimulation

One day following surgery, mice began an adaptation procedure, receiving a constant influx of filtered water through the intraoral cannula (0.15 ml/min for 15 min) using a precision syringe pump (model 341A; Sage Instruments, Cambridge, MA, USA) in a round Plexiglas test chamber (11.5 cm diameter, 14.5 cm height). This training occurred at roughly the same time (between 1300 h and 1500 h) for three consecutive days prior to the test day. Mice were then food and water restricted 20 h prior to testing, to promote sampling of stimuli, and to ensure mice had not consumed a meal in their home cage prior to testing. A recent study by Stratford and Thompson (2016) in mice demonstrated that the use of water restriction prior to testing, and constant stimulation through the IO cannula, produced Fos expression in the NST similar to that evoked by consumption from a bottle.

On the test day, mice were placed in the test chamber at the same time of day as the adaptation procedure. For the next 15 minutes, mice were intraorally infused with 2.25 ml of one of the following stimuli using the same methods and rate used in the adaptation procedure: Filtered water (n = 4), 0.5 M sucrose (n = 6), or 0.003 M QHCl (n = 4). Solutions of sucrose (Fisher Scientific) and quinine HCl (Sigma Aldrich) were prepared just prior to use. The concentrations were the same as in our previous study, which used a similar paradigm (Tokita et al., 2014). Following testing, mice were returned to home cages and given no additional food or water before perfusion.

4.4. Histology, histochemistry, and immunofluorescence

In the anterograde experiment, mice were perfused after a 7–10 day survival period. In the retrograde experiment, mice were perfused 2 hours after the onset of the taste stimulation. All mice were perfused transcardially with 0.02 M phosphate-buffered physiological saline (PBS) followed by ice-cold 4% paraformaldehyde in 0.1 M phosphate buffer. The brains were removed and postfixed in 4% paraformaldehyde for 1 day, and then transferred to a 30% buffered sucrose solution for cryoprotection and stored at 4°C for at least 1 week. Coronal brain sections (40 μm) were cut serially using a freezing microtome and divided

into two adjacent series. One series was Nissl-stained with cresyl violet to reveal cytoarchitecture, and the adjacent series was used for examination of tracer injection sites and neuronal labeling.

For visualizing BDA, sections were rinsed, followed by pretreatment with 3% H_2O_2 and 0.4% Triton X-100 (Sigma-Aldrich, St. Louis, MO, USA). Sections were then rinsed again and incubated in avidin-biotin complex (ABC) solution prepared with the Vectastain ABC Elite kit (Vector Laboratories, Burlingame, CA). BDA appeared as a black reaction product using nickel intensification of the chromagen, 3,3'-diaminobenzidine (DAB; Vector). The sections were then rinsed, mounted, air-dried, and coverslipped with mounting medium DPX (Fluka, Milwaukee, WI, USA) for bright field microscopy.

Microruby is a rhodamine conjugate that is detectable with fluorescence microscopy using a TRITC filter, so no other procedures were necessary to visualize anterograde labeling in sections from these mice. For staining of tyrosine hydroxylase (TH) in the microruby-injected mice, the following immunofluorescence protocol was used: Sections were first rinsed in PBS, and then incubated (blocking step) in 3% normal donkey serum (NDS; Jackson ImmunoResearch Laboratories, West Grove, PA, USA) for 30 minutes. After rinsing in PBS, sections were incubated with primary antibody (mouse anti-TH; 1:5000, ImmunoStar, Hudson, WI, USA) in PBS containing 3% NDS and 0.5% triton X-100 for 48 h at 4°C. Several sections were placed in the same solution only lacking the primary antibody to serve as a negative control. Sections were then rinsed and blocked again in 3% NDS for 30 min, followed by incubation for 2 h with the secondary antibody: Biotinylated donkey anti-rabbit IgG (1:1000, Jackson ImmunoResearch Laboratories, West Grove, PA, USA) in PBS containing 3% NDS and 0.5% triton X-100. Sections were then rinsed and transferred to streptavidin-Cy2 (Jackson ImmunoResearch) diluted to a concentration of 1:1000 in PBS for 1 h. Finally, sections were rinsed, mounted on slides, and coverslipped with mounting medium Vectashield (Vector Laboratories, Burlingame, CA, USA) for fluorescence microscopy. No TH immunoreactivity was observed in control sections.

CTb and Fos were visualized using a very similar immunofluorescence protocol (FG fluoresces under UV light, so no further processing was required for visualization). The protocol was the same as for TH, including the length of each step, with the following differences: A cocktail of 2 primary antibodies was used, including goat anti-CTb (1:5000, List Biological Laboratories, Campbell, CA, USA) and rabbit anti-c-Fos (1:5000, Santa Cruz Biotechnology, CA, USA) in PBS containing 3% NDS and 0.5% triton X-100. Similarly, a cocktail of 2 secondary antibodies was used: FITC-conjugated donkey anti-goat IgG (1:500; Jackson ImmunoResearch) and biotinylated donkey anti-rabbit IgG (1:1000, Jackson ImmunoResearch) in PBS containing 3% NDS and 0.5% triton X-100 for 2 h. The final incubation step used streptavidin-Cy3 (Jackson ImmunoResearch Laboratories) diluted to a concentration of 1:1000 in PBS. No CTb or Fos immunoreactivity was observed in no-primary antibody control sections.

4.5 Microscopic analysis of sections

For anterograde tracing with BDA, brain sections were examined via light microscopy (Leica DMRXA2, Leica Microsystems, Bannockburn, IL, USA) for axonal and terminal

labeling. Every other section was examined from the start of the PBN (about 5.7 mm posterior to bregma) to the posterior insular cortex (about 0.0 bregma). Because the afferent projections from PBN have been relatively well-described (although predominantly in rats), this analysis was strictly qualitative in nature, with an experienced experimenter (J.B.) noting the presence and relative amount of label in the VTA and in other known projection fields. Representative images were collected using a digital camera (Hamamatsu ORCA-ER, Hamamatsu Photonics, Shizuoka, Japan) and imaging software (SimplePCI, Hamamatsu Photonics, Shizuoka, Japan) connected to the microscope. For anterograde tracing with microruby, and for the retrograde tracing experiments, fluorescent microscopy (using the same microscope, camera and imaging software) was used. In addition, some brain sections were imaged using a confocal microscope (Zeiss 710, Carl Zeiss, Thornwood, NY) to show high-magnification examples of immunofluorescent labeling.

In the retrograde tracing experiment, FG and CTb injection sites (in the VTA and VPMpc, respectively) were imaged under fluorescence at 5X, outlined, and plotted onto a standard schematic template. The area (in pixels) within each outline was calculated using the measurement tool in Adobe Photoshop CS5 (Adobe Systems Inc., San Jose, CA). In the PBN, estimates of numbers of fluorescently labeled cells (FG, CTb and Fos) were made by a single, experienced observer (J.B.), blind to the stimulus condition. Cells were counted from high-resolution 10X and 20X (depending on subnucleus and label density) digital microscopic images using ImageJ 1.48v (National Institutes of Health, USA). Delineation of nine PBN subnuclei was made with the use of cresyl violet-stained sections (Fig. 1), according to our previous anatomical studies in the mouse (Tokita et al., 2010; 2014), which in turn were based on the histological delineation of Hashimoto et al. (2009). Labeled cells in the PBN were quantified on both sides of the brain in 5 sequential sections along the rostral-caudal axis. This span of sections, spaced evenly over 360 μm, fits approximately within a length (400 μm) of the pons corresponding to images 106–110 of the coronal mouse brain reference atlas at Allen Brain Atlas (–5.26 to –5.66 mm relative to bregma). Based on the aforementioned studies, as well as our spatial plots of taste-responsive neurons (using *in vivo* electrophysiology) we are confident this range captures the majority of taste-elicited activity in the mouse PBN, which tends to be found at more caudal levels (Hashimoto et al., 2009; Tokita et al., 2014; 2016; Li and Lemon, 2018).

Each type of cell was initially counted from a single channel color image. Only complete or nearly complete cellular (FG, CTb labeling; PBN cells are predominantly round, oval, or fusiform) or nuclear (Fos) profiles were counted. Moreover, peak intensity of the profile had to exceed the average background intensity, which was determined for each image from a 300 X 300 pixel ROI placed over a cell-containing but non-PBN region of the brainstem within that image. Double-labeled and triple-labeled cells were counted using merged images.

4.6 Statistical analysis

Statistical analyses for cell counts (FG, CTb, Fos, and double-labeled cells) were performed using SPSS v.25 (IBM Corp. Armonk, NY) and were guided by several *a priori* hypotheses for this experiment. First, we expected that counts of either type of tracer-labeled cell (FG or

CTb) would not vary among stimulus groups. This hypothesis was based on there being no reason to believe that IO stimulation, performed just before perfusion, would affect retrograde transport and expression of tracers. Secondly, we hypothesized that numbers of Fos-IR cells would not vary according to brain side; this hypothesis was based on our previous intraoral-evoked Fos expression study in the mouse PBN (Tokita et al., 2014). These hypotheses were confirmed (i.e., lack of effects) in omnibus 3-way mixed ANOVAs conducted on cell counts of each type. Therefore, for examining FG and CTb cell counts, data were combined into a single group (n = 14) for better statistical power and examined with respect to side and subnucleus. For Fos-IR cells, counts were averaged across side and examined with respect to stimulus (n = 4–6) and subnucleus. No specific hypotheses were made concerning the distribution of each type of double-labeled (DL) cell. However, DL cells were not found in all subnuclei. For parametric analysis DL cells were summed across subnuclei within the medial and lateral regions of the PBN and examined with respect to stimulus, region, and side.

Prior to analysis, cell count data were examined for normality (Shapiro-Wilk test), and homogeneity of variance (Levene's test) where appropriate (i.e., between stimulus groups). The majority of data cells passed these tests: 75–100% (per analysis) for normality, and 75–89% for homogeneity of variance. Based on the results of these assumption tests, we cautiously proceeded with parametric analyses. For within-subjects factors, a Greenhouse-Geiser correction for violation of sphericity was also used where needed. Where indicated, post-hoc comparisons were made with Tukey's test ($p < 0.05$).

Acknowledgements

The authors gratefully acknowledge the assistance and helpful comments of William E. Armstrong and Max Fletcher. This research was supported by National Institutes of Health grant NIHDC000353 (J.D.B.).

References

Bachmanov AA, Tordoff MG, Beauchamp GK (2001). Sweetener preference of C57BL/6ByJ and 129P3/J mice. Chem Senses, 26, 905–913. [PubMed: 11555485]

Bamji-Stocke S, Biggs BT, Samuelsen CL (2018) Experience-dependent c-Fos expression in the primary chemosensory cortices of the rat. Brain Res, 1701, 189–195. [PubMed: 30244018]

Bassareo V, De Luca AM, Di Chiara G (2002) Differential Expression of Motivational Stimulus Properties by Dopamine in Nucleus Accumbens Shell versus Core and Prefrontal Cortex. J. Neurosci 22, 4709–4719. [PubMed: 12040078]

Beier KT, Steinberg EE, DeLoach KE, Xie S, Miyamichi K, Schwarz L, Gao XJ, Kremer EJ, Malenka RC, Luo L. (2015) Circuit Architecture of VTA Dopamine Neurons Revealed by Systematic Input-Output Mapping. Cell 162:622–34. [PubMed: 26232228]

Berridge KC, Kringelbach ML. (2008) Affective neuroscience of pleasure: reward in humans and animals. Psychopharmacology 199:457–80. [PubMed: 18311558]

Berridge KC, Kringelbach ML. (2015) Pleasure Systems in the Brain. Neuron 86, 646–664. [PubMed: 25950633]

Berridge KC (2007). The debate over dopamine's role in reward: the case for incentive salience. Psychopharmacology 191:391–431. [PubMed: 17072591]

Boughter JD, Raghow S, Nelson TM, Munger SD (2005). Inbred mouse strains C57BL/6J and DBA/2J vary in sensitivity to a subset of bitter stimuli. BMC Genet, 6, 36. [PubMed: 15967025]

Brischoux F, Chakraborty S, Brierly DI, Ungless MA (2009) Phasic excitation of dopamine neurons in ventral VTA by noxious stimuli. Proc. Nat. Acad Sci 106, 4894–4899. [PubMed: 19261850]

Brog JS, Salyapongse A, Deutch AY, Zahm DS. (1993) The patterns of afferent innervation of the core and shell in the “accumbens” part of the rat ventral striatum: immunohistochemical detection of retrogradely transported fluoro-gold. J Comp Neurol 338:255–78. [PubMed: 8308171]

Carter ME, Soden ME, Zweifel LS, and Palmiter RD (2013). Genetic identification of a neural circuit that suppresses appetite. Nature 503, 111–114. [PubMed: 24121436]

Campos CA, Bowen AJ, Roman CW, Palmiter RD (2018). Encoding of danger by parabrachial CGRP neurons. Nature 555:617–622. [PubMed: 29562230]

Cassell MD, Freedman LJ, Shi C. (1999) The intrinsic organization of the central extended amygdala. Ann N Y Acad Sci 877:217–41. [PubMed: 10415652]

Chaudhari N, Roper SD (2010) The cell biology of taste. Journal of Cell Biology 190, 285–296. [PubMed: 20696704]

Coizet V, Dommett EJ, Klop EM, Redgrave P, Overton PG. (2010) The parabrachial nucleus is a critical link in the transmission of short latency nociceptive information to midbrain dopaminergic neurons. Neuroscience 168:263–72. [PubMed: 20363297]

Dela Cruz JAD, Coke T, Bodnar RJ (2016) Simultaneous Detection of c-Fos Activation from Mesolimbic and Mesocortical Dopamine Reward Sites Following Naive Sugar and Fat Ingestion in Rats. J Vis Exp 114, e53897.

D’Hanis W, Linke R, Yilmazer-Hanke DM (2007) Topography of Thalamic and Parabrachial Calcitonin Gene-Related Peptide (CGRP) Immunoreactive Neurons Projecting to Subnuclei of the Amygdala and Extended Amygdala. J Comp. Neurol 505, 268–291. [PubMed: 17879271]

Dotson CD, Spector AC (2007). Behavioral discrimination between sucrose and other natural sweeteners in mice: Implications for the neural coding of T1R ligands. J. Neurosci, 27, 11242–11253 [PubMed: 17942718]

Douglass AM et al. (2017) Central amygdala circuits modulate food consumption through a positive-valence mechanism. Nat. Neurosci 20, 1384–1394 [PubMed: 28825719]

Fenelon JD, Poulain DA, Theodosis DT. (1993) Oxytocin neuron activation and fos expression: a quantitative immunocytochemical analysis of the effect of lactation, parturition, osmotic and cardiovascular stimulation. Neuroscience 53, 77–89. [PubMed: 8469314]

Figlewicz DP, Bennett-Jay JL, Sipols AJ, Zavosh A (2011) Sucrose self-administration and CNS activation in the rat. Am J Physiol Regul Integr Comp Physiol 300, R876–R884. [PubMed: 21307361]

Franklin TR, Druhan JP. (2000) The retrograde tracer fluoro-gold interferes with the expression of fos-related antigens. J Neurosci Methods 98, 1–8. [PubMed: 10837865]

Fulwiler CE, Saper CB. (1984) Subnuclear organization of the efferent connections of the parabrachial nucleus in the rat. Brain Res 319:229–59. [PubMed: 6478256]

Garfield AS et al. (2015) A neural basis for melanocortin-4 receptor-regulated appetite. Nat. Neurosci 18, 863–872 [PubMed: 25915476]

Gauriau C and Bernard J-F (2001) Pain pathways and parabrachial circuits in the rat. Exp. Physiol 87, 251–258

Hajnal A, Norgren R. (2001) Accumbens dopamine mechanisms in sucrose intake. Brain Res 904:76–84. [PubMed: 11516413]

Hajnal A, Smith GP, Norgren R. (2004) Oral sucrose stimulation increases accumbens dopamine in the rat. Am J Physiol Regul Integr Comp Physiol 286:R31–7 [PubMed: 12933362]

Halsell CB. (1992) Organization of parabrachial nucleus efferents to the thalamus and amygdala in the golden hamster. J Comp Neurol 317:57–78. [PubMed: 1374087]

Han S et al. (2015) Elucidating an affective pain circuit that creates a threat memory. Cell 162, 363–374 [PubMed: 26186190]

Hashimoto K, Obata K, Ogawa H. (2009) Characterization of parabrachial subnuclei in mice with regard to salt tastants: possible independence of taste relay from visceral processing. Chem Senses 34:253–67. [PubMed: 19179538]

Jin J, Maren S (2015) Fear renewal preferentially activates ventral hippocampal neurons projecting to both amygdala and prefrontal cortex in rats. Sci Reports 5:8388.

Kang N, McCarthy EA, Cherry JA, Baum MJ (2011) A sex comparison of the anatomy and function of the main olfactory bulb-medial amygdala projection in mice. Neuroscience 172:196–204. [PubMed: 21070839]

Karimnamazi H, Travers JB. (1998) Differential projections from gustatory responsive regions of the parabrachial nucleus to the medulla and forebrain. Brain Res 813:283–302. [PubMed: 9838165]

Karimnamazi H, Travers SP, Travers JB. (2002) Oral and gastric input to the parabrachial nucleus of the rat. Brain Res 957:193–206. [PubMed: 12445962]

King CT, Deyrup LD, Dodson SE, Galvin KE, Garcea M, Spector AC (2003) Effects of gustatory nerve transection and regeneration on quinine-stimulated Fos-like immunoreactivity in the parabrachial nucleus of the rat. J Comp Neurol 465:296–308. [PubMed: 12949788]

Kovács KJ. (2008). Measurement of immediate-early gene activation- c-fos and beyond. J Neuroendocrinol 20(6):665–72. [PubMed: 18601687]

Krukoff TL, Harris KH, Jhamandas JH. (1993) Efferent projections from the parabrachial nucleus demonstrated with the anterograde tracer Phaseolus vulgaris leucoagglutinin. Brain Res Bull 30:163–72. [PubMed: 7678381]

Li CS, Chung S, Lu DP, Cho YK. (2012) Descending projections from the nucleus accumbens shell suppress activity of taste-responsive neurons in the hamster parabrachial nuclei. J Neurophysiol 108:1288–98. [PubMed: 22696536]

Lu YC et al. (2015) Neurochemical properties of the synapses between the parabrachial nucleus-derived CGRP-positive axonal terminals and the GABAergic neurons in the lateral capsular division of central nucleus of amygdala. Mol. Neurobiol 51, 105–118 [PubMed: 24794145]

Li J, Lemon CH (2019) Mouse parabrachial neurons signal a relationship between bitter taste and nociceptive stimuli. J. Neurosci. doi: 10.1523/JNEUROSCI.2000-18.2018. [Epub ahead of print].

Mark GP, Blander DS, Hoebel BG. (1991). A conditioned stimulus decreases extracellular dopamine in the nucleus accumbens after the development of a learned taste aversion. Brain Res 551:308–10. [PubMed: 1913157]

Martinez-Hernandez J, Lanuza E, Martinez-Garcia F (2006) Selective dopaminergic lesions of the ventral tegmental area impair preference for sucrose but not for male sexual pheromones in female mice. Euro. J Neurosci 24, 885–893.

Monroe S, Di Lorenzo PM. (1995) Taste responses in neurons in the nucleus of the solitary tract that do and do not project to the parabrachial pons. J Neurophysiol 74:249–57. [PubMed: 7472328]

Mungarndee SS, Lundy RF Jr, Norgren R. (2008) Expression of Fos during sham sucrose intake in rats with central gustatory lesions. Am J Physiol Regul Integr Comp Physiol 295:R751–63. [PubMed: 18635449]

Nieh EH, Matthews GA, Allsop SA, Presbrey KN, Leppla CA, Wichmann R, Neve R, Wildes CP, Tye KM. (2015) Decoding neural circuits that control compulsive sucrose seeking. Cell, 160:528–41. [PubMed: 25635460]

Norgren R, Leonard CM. (1973) Ascending central gustatory pathways. J Comp. Neurol, 150, 217–237. [PubMed: 4723066]

Ogawa H, Hayama T, Ito S (1987) Response properties of the parabrachio-thalamic taste and mechanoreceptive neurons in rats. Exp Brain Res 68:449–57. [PubMed: 3691718]

Palmiter RD (2018) The Parabrachial Nucleus: CGRP Neurons Function as a General Alarm. Trends Neurosci 41, 280–293. [PubMed: 29703377]

Park TH, Carr KD (1998) Neuroanatomical patterns of Fos-like immunoreactivity induced by a palatable meal and meal-paired environment in saline- and naltrexone-treated rats. Brain Res 805, 169–180. [PubMed: 9733960]

Phillipson OT. (1979) Afferent projections to the ventral tegmental area of Tsai and interfascicular nucleus: a horseradish peroxidase study in the rat. J Comp Neurol 187:117–43. [PubMed: 489776]

Norgren R, Leonard CM. (1973) Ascending central gustatory pathways. J Comp Neurol 150:217–37. [PubMed: 4723066]

Norgren R (1974) Gustatory afferents to ventral forebrain. Brain Res 81:285–95. [PubMed: 4434198]

Norgren R (1978) Projections from the nucleus of the solitary tract in the rat. Neuroscience 3:207–218 [PubMed: 733004]

Riley CA, King MS (2013) Differential effects of electrical stimulation of the central amygdala and lateral hypothalamus on fos-immunoreactive neurons in the gustatory brainstem and taste reactivity behaviors in conscious rats. Chem Senses 38:705–17. [PubMed: 23978688]

Roman CW, Derkach VA, Palmiter RD (2015). Genetically and functionally defined NTS to PBN brain circuits mediating anorexia. Nature Commun 7, 11905.

Sanchez-Catalan MJ, Kaufling J, Georges F, Veinante P, Barrot M (2014). The antero-posterior heterogeneity of the ventral tegmental area. Neurosci, 282: 198–216.

Saper CB, Loewy AD. (1980) Efferent connections of the parabrachial nucleus in the rat. Brain Res 197:291–317. [PubMed: 7407557]

Shibata R, Kameishi M, Kondoh T, Torii K (2009) Bilateral dopaminergic lesions in the ventral tegmental area of rats influence sucrose intake, but not umami and amino acid intake. Physiol. Behav 96, 667–674. [PubMed: 19174174]

Shultz W, Dayan P, Montague PR (1997) A neural substrate of prediction and reward. Science, 275: 1593–1599. [PubMed: 9054347]

Shimura T, Kamada Y, Yamamoto T (2002). Ventral tegmental lesions reduce overconsumption of normally preferred taste fluid in rats. Behav Brain Res 134: 123–130. [PubMed: 12191798]

Stratford JM, Thompson JA (2016) MSG-evoked c-Fos activity in the nucleus of the solitary tract is dependent upon fluid delivery and stimulation parameters. Chem. Senses, 41: 211–220. [PubMed: 26762887]

Takahashi YK, Batchelor HM, Liu B, Khanna A, Morales M, Schoenbaum G (2017) Dopamine Neurons Respond to Errors in the Prediction of Sensory Features of Expected Rewards. Neuron 95, 1395–1405. [PubMed: 28910622]

Tan KR, Yvon C, Turiault M, Mirzabekov JJ, Doehner J, Labouèbe G, Deisseroth K, Tye KM, Lüscher C (2012) GABA neurons of the VTA drive conditioned place aversion. Neuron, 73, 1173–83. [PubMed: 22445344]

Tellez LA, Han W, Zhang X, Ferreira TL, Perez IO, Shammah-Lagnado SJ, van den Pol AN, de Araujo IE. (2016). Separate circuitries encode the hedonic and nutritional values of sugar. Nat Neurosci 19:465–70. [PubMed: 26807950]

Tokita K, Shimura T, Nakamura S, Inoue T, Yamamoto T (2007) Involvement of forebrain in parabrachial neuronal activation induced by aversively conditioned taste stimuli in the rat. Brain Res 1141:188–96. [PubMed: 17276421]

Tokita K, Inoue T, Boughter JD Jr. (2009) Afferent connections of the parabrachial nucleus in C57BL/6J mice. Neuroscience 161:475–88. [PubMed: 19327389]

Tokita K, Inoue T, Boughter JD Jr. (2010) Subnuclear organization of parabrachial efferents to the thalamus, amygdala and lateral hypothalamus in C57BL/6J mice: a quantitative retrograde double labeling study. Neuroscience 171:351–65. [PubMed: 20832453]

Tokita K, Armstrong W St., John SJ, Boughter JD Jr. (2014) Activation of lateral hypothalamus-projecting parabrachial neurons by intraorally delivered gustatory stimuli. Front. Neural Circuits 8:86. [PubMed: 25120438]

Tokita K, Boughter JD Jr. (2016) Topographic organizations of taste-responsive neurons in the parabrachial nucleus of C57BL/6J mice: An electrophysiological mapping study. Neuroscience 316:151–166 [PubMed: 26708748]

Travers SP, Hu H (2000) Extranuclear projections of rNST neurons expressing gustatory-elicited Fos. J Comp. Neurol, 427:124–138. [PubMed: 11042595]

Ungless M (2004) Dopamine: the salient issue. Trends Neurosci 27, 702–706. [PubMed: 15541509]

Voshart K, van der Kooy D. (1981) The organization of the efferent projections of the parabrachial nucleus of the forebrain in the rat: a retrograde fluorescent double-labeling study. Brain Res 212:271–86. [PubMed: 7225869]

Watabe-Uchida M, Zhu L, Ogawa SK, Vamanrao A, Uchida N. (2012) Whole-brain mapping of direct inputs to midbrain dopamine neurons. Neuron 74:858–73. [PubMed: 22681690]

Yamamoto T, Shimura T, Sako N, Sakai N, Tanimizu T, Wakisaka S (1993) c-Fos expression in the parabrachial nucleus after ingestion of sodium chloride in the rat. Neuroreport 4:1223–6. [PubMed: 8219018]

Yamamoto T, Shimura T, Sakai N, Ozaki N (1994) Representation of hedonics and quality of taste stimuli in the parabrachial nucleus of the rat. Physiol Behav 56:1197–202. [PubMed: 7878091]

Yamamoto T, Sawa K (2000) Comparison of c-fos-like immunoreactivity in the brainstem following intraoral and intragastric infusions of chemical solutions in rats. Brain Res 866:144–51. [PubMed: 10825490]

Yamamoto T (2006) Neural substrates for the processing of cognitive and affective aspects of taste in the brain. Arch Histol Cytol 69:243–55. [PubMed: 17287579]

Yokota S, Kaur S, VanderHorst VG, Saper CB, Chamberlin NL. (2015) Respiratory-related outputs of glutamatergic, hypercapnia-responsive parabrachial neurons in mice. J Comp Neurol 523:907–20. [PubMed: 25424719]

Highlights:

- A subset of brainstem taste neurons project to an important midbrain reward area
- This projection is independent from the thalamo-cortical pathway
- These neurons carry information about both sweet and bitter taste

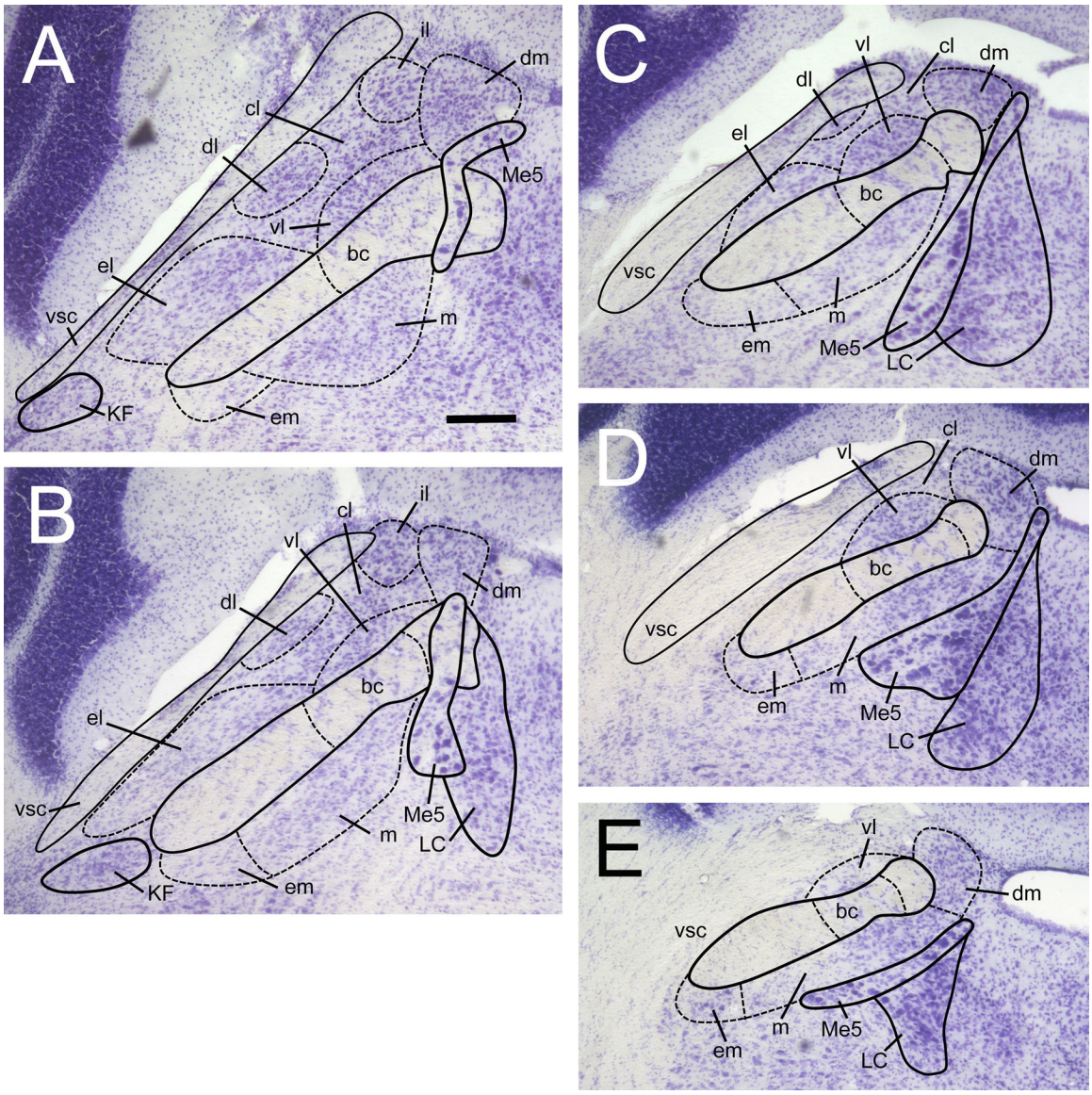

Figure 1.

Delineation of the PBN at 5 levels along the rostral-caudal axis of the mouse brain. Sections were nissl-stained with cresyl violet to reveal cytoarchitecture. This span of sections (40 μm thickness) is spaced out evenly over a 360 μm distance, starting at the most rostral section (A), approximately –5.24 mm relative to bregma. Sections are ordered A-E, from rostral to most caudal. PBN subnuclei are labeled as follows: dm, dorsal medial; m, medial; em, external medial; bc, brachium conjunctivum; vl, ventral lateral; cl, central lateral; dl, dorsal lateral; el, external lateral; il, internal lateral. All pictures at same magnification, scale bar in A = 100 μm. Other abbreviations are: vsc, ventral spinocerebellar tract; Me5, mesencephalic trigeminal nucleus; LC, locus coeruleus; KF, kolliker-fuse nucleus.

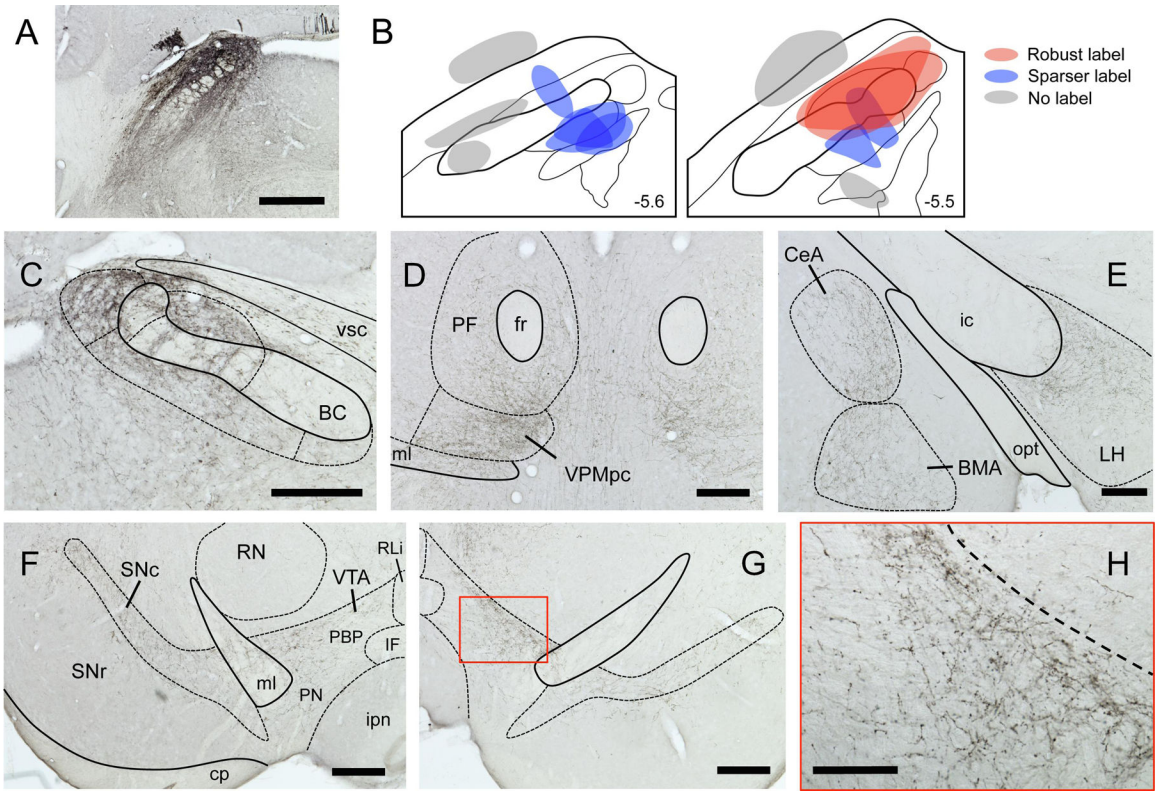

Figure 2.

Anterograde tracing from PBN reveals projections to taste-associated brain areas. A. Representative image of BDA tracer injection site into caudal PBN. B. Approximate injection sites for 13 mice; those injections that infiltrated primarily lateral but also medial regions of PBN (red) produced the most robust label in upstream brain regions. Smaller, more restricted injections (blue) produced sparser labeling, while off-target injections (gray) produced no labeling. Characteristic terminal labeling is shown in the contralateral PBN (C), bilaterally in the medial thalamus (D), ipsilaterally in the amygdala and LH, and bilaterally in the SNc and VTA (F-G). VTA level is approximately - 3.2 mm from Bregma. Higher magnification view of contralateral VTA (red box in G) is shown in H. All micrographs are from a single animal. Delineations based on Allen Brain Atlas. Scale bars: A = 500 μm, C-G = 250 μm, H = 100 μm. Abbreviations in panel F delineating VTA subregions: PBP, parabrachial pigmented nucleus; PN, paranigral nucleus; IF, interfasicular nucleus; RLi, rostral linear nucleus.

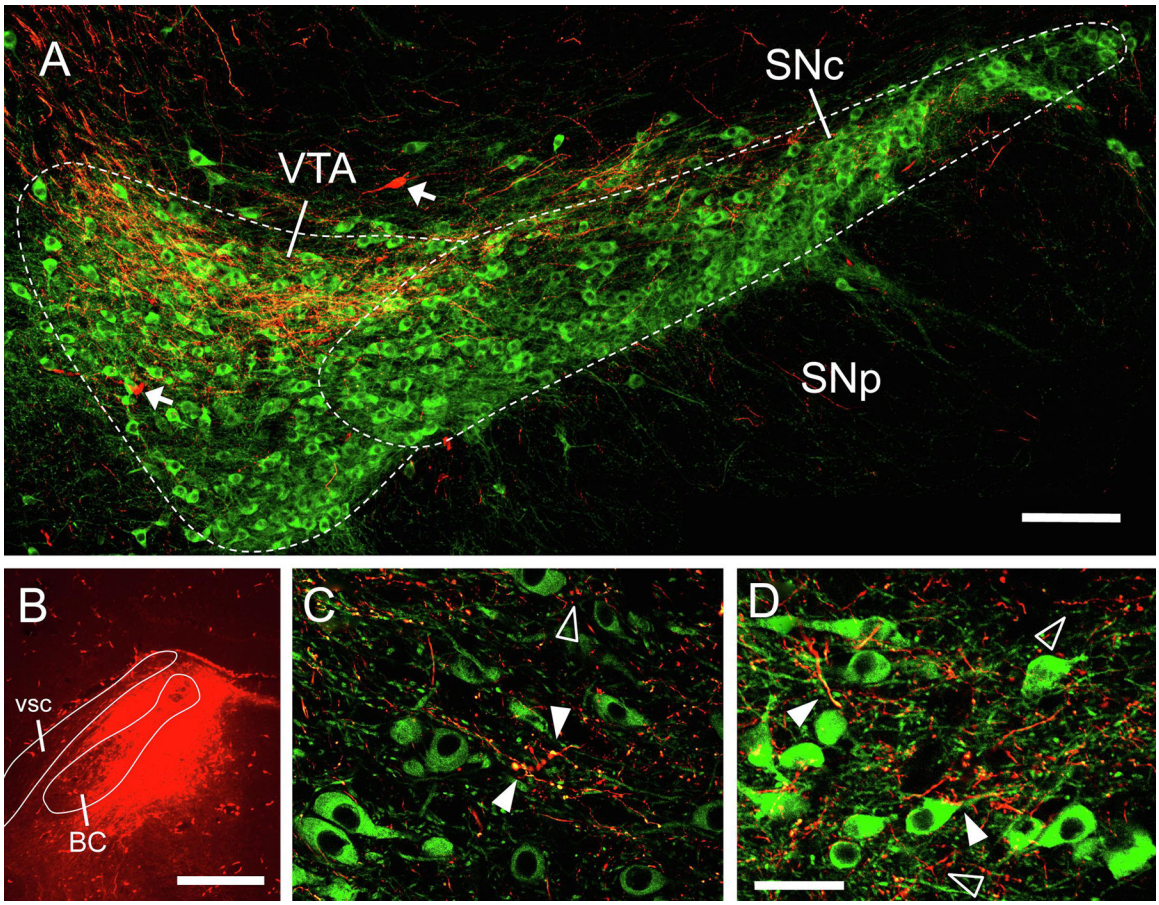

Figure 3.

Anterograde labeling from PBN in proximity to TH+ neurons in the contralateral VTA and SNc. A. lower power image shows fibers and terminals from PBN (red) intermingling with TH+ neurons, especially in the dorsal field of the VTA. Arrows show examples of retrogradely-labeled neurons. B. tracer injection site in the PBN. C-D. Higher magnification images (same animal as A, but different images) show areas of overlap between anterograde-labeled terminal processes (red) and TH+ cell bodies and dendritic processes (green – examples of overlap indicated by solid arrowheads). In other places, terminal processes do not overlap with TH+ elements (open arrowheads). AP level in VTA images approximately −2.8 mm from bregma, delineation based on Allen Brain Atlas. Scale bars: A = 100 μm, B = 500 μm, C-D = 20 μm.

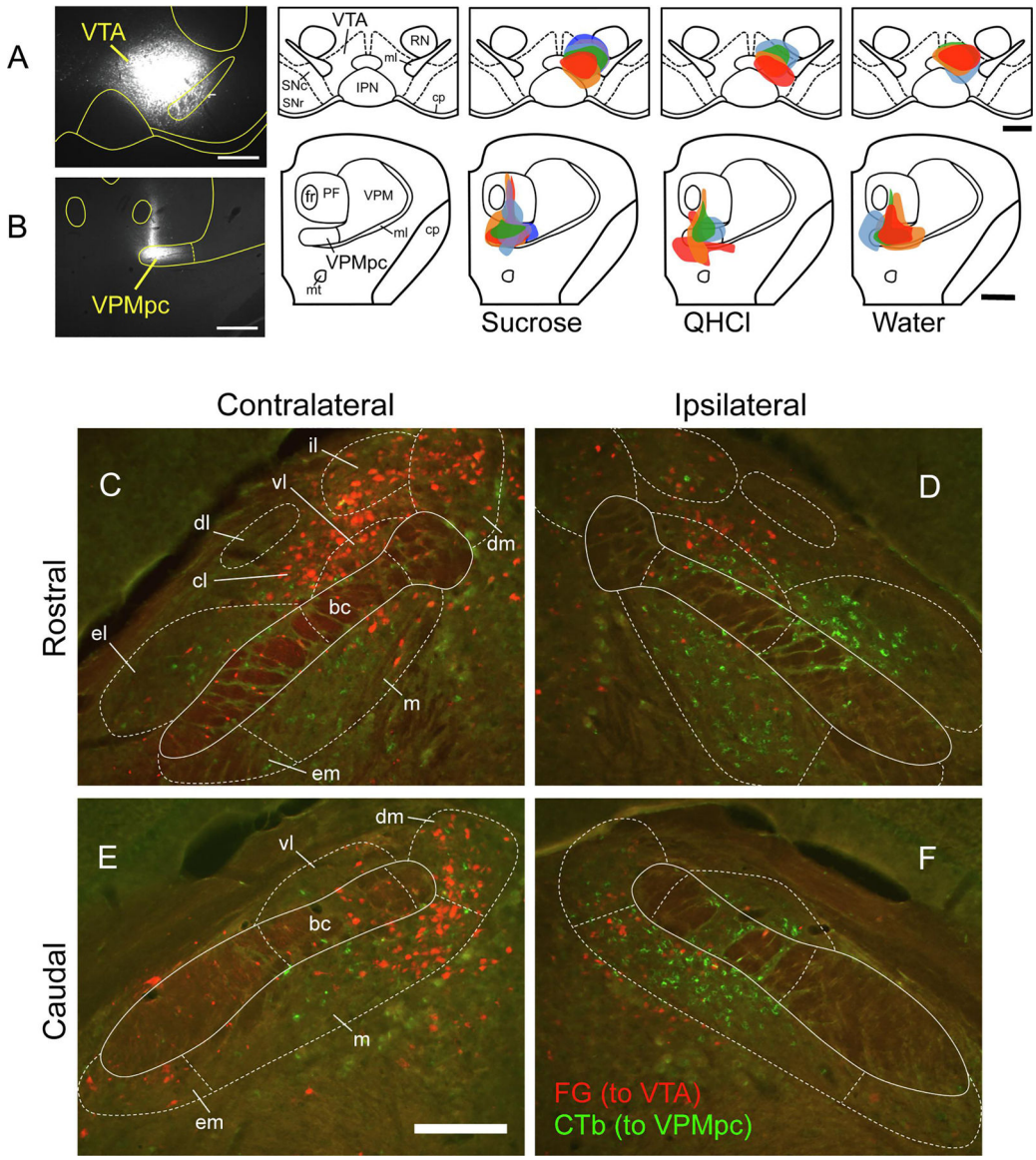

Figure 4.

VTA and VPMpc injection sites, and neuronal cell body labeling in the PBN. A. Representative photomicrograph of VTA injection site, and plots of injection site and size in the VTA for each animal according to stimulus group. B. Representative photomicrograph of VPMpc injection site, and plots of injection site and size in the VPMpc for each animal according to stimulus group. Colors identify single animals within each group, consistent for injections at both brain sites. C-F: Tracer labeling in the PBN. Low-power (10X) Fluorescent images taken from both sides of 2 brain sections from a single mouse, with rostral (top) and caudal (bottom) levels of the PBN shown. Retrograde FG labeling (red) from the VTA was stronger on the contralateral side, whereas retrograde CTb labeling (green) was stronger on the ipsilateral side. In these images, Fos-IR cells are not shown. Scale bars: A-B = 500 μm, E = 200 μm.

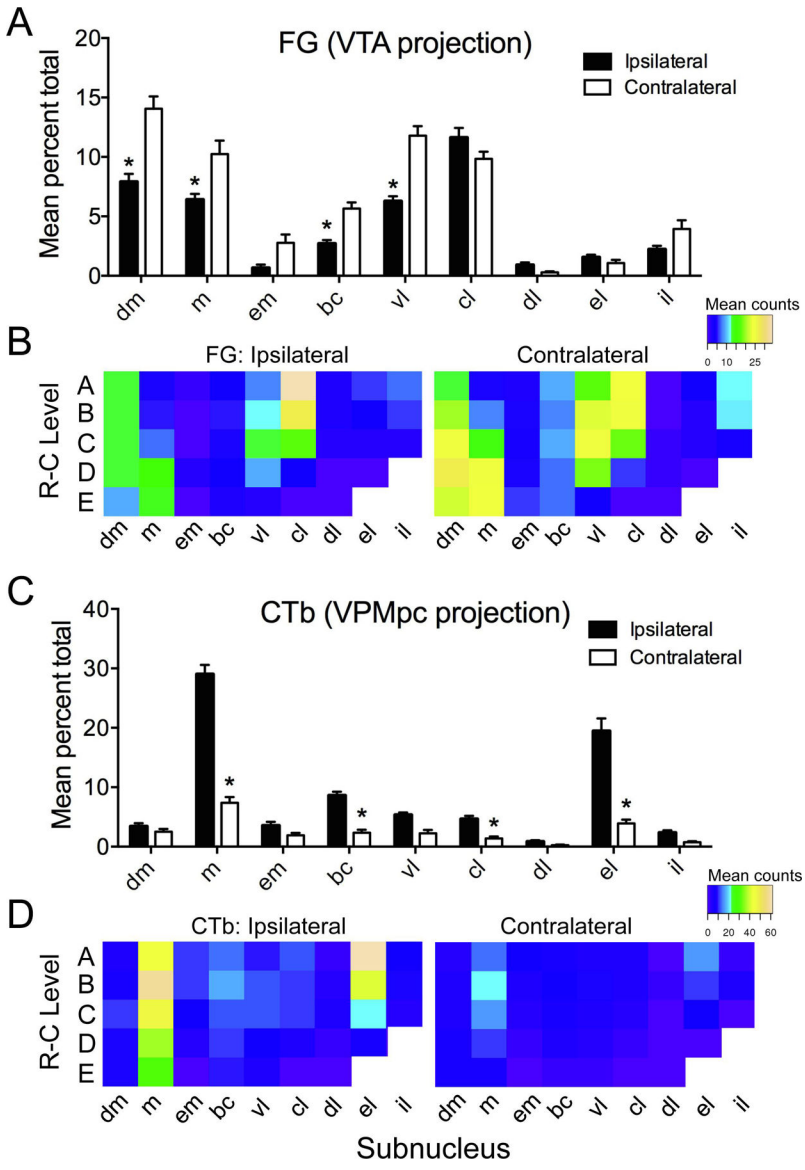

Figure 5.

Quantification of FG and CTb retrogradely-labeled cells in the PBN by subnucleus and according to rostral-caudal (RC) level. A. Mean number (expressed as % of total) of FG (VTA-projecting) neurons, combined across stimulus groups, varied according to both subnuclear location and side of the brain. B. Heat maps show relative numbers of FG-labeled cells in each subnucleus at each of 5 RC levels on either side. C-D. Similar plots and heat maps are shown for CTb (VPMpc-projecting) neurons. Asterisks in A,C show significant ipsilateral-contralateral differences in particular subnuclei ($p < 0.05$).

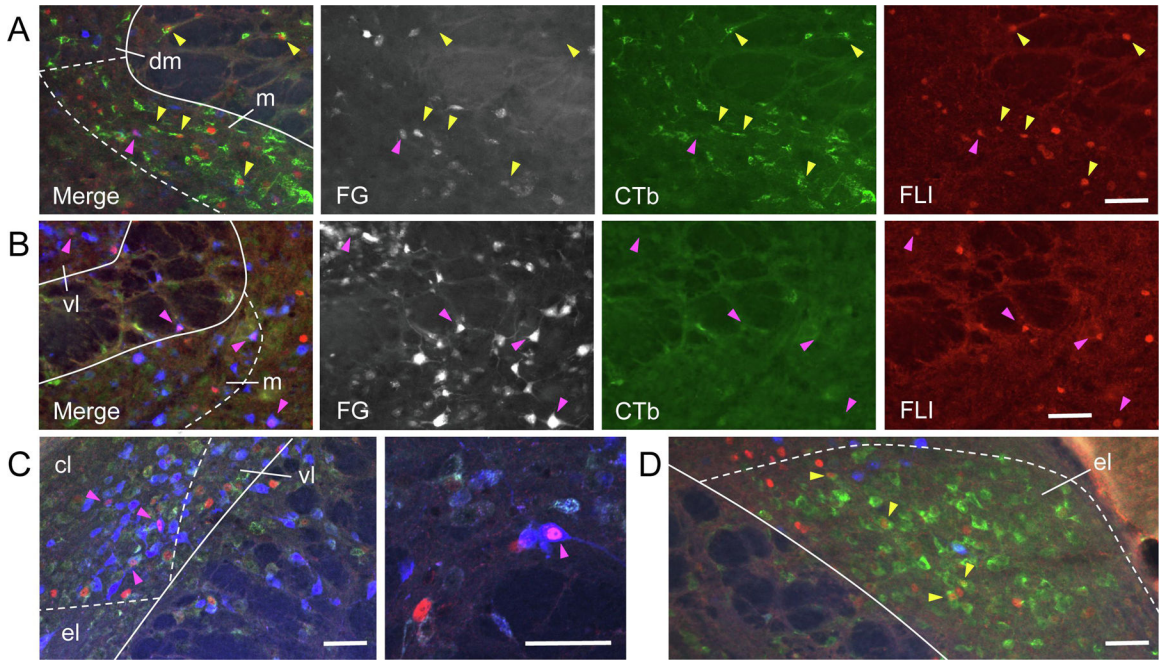

Figure 6.

Examples of FG, CTb, and FLI (Fos-like immunoreactivity) labeling in the PBN, shown as both merged images, as well as individual channels for each fluorophore (FG, colored blue in the merged image, is shown more clearly in grayscale). A. Several cells doubled-labeled for CTb and sucrose-evoked FLI (yellow arrowheads) are found in the ipsilateral, caudal PBN in the medial (m) subnucleus. B. Cells double-labeled for FG and sucrose-evoked FLI (pink arrowheads) in m and ventral lateral (vl) subnuclei on the contralateral side in a more rostral level of the PBN. C. Cells double-labeled for FG and quinine-evoked FLI in the central lateral (cl) subnucleus in the contralateral, rostral PBN; High-magnification image from same animal shown in second panel. D. Robust expression of CTb and sucrose-evoked FLI in the ipsilateral external lateral (el) subnucleus. Scale bars = 100 μm.

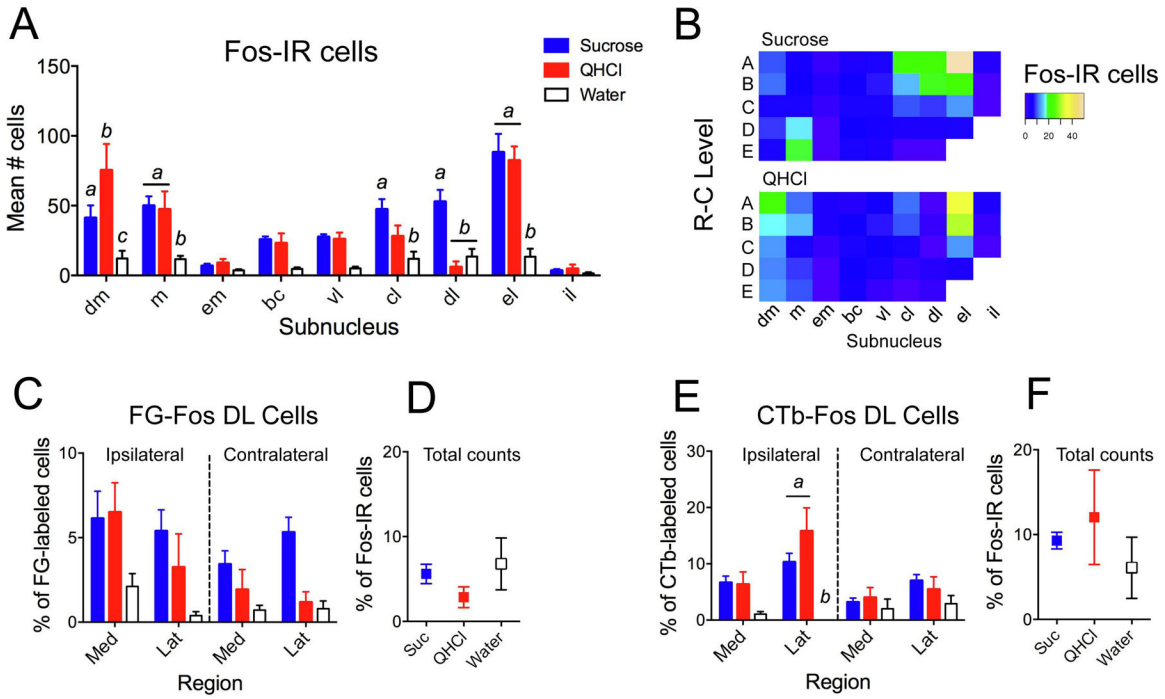

Figure 7.

Quantification of Fos-IR and double-labeled (DL) cells. A. Mean number of Fos-IR cells according to stimulus and subnucleus. B. Heat maps show relative number of Fos-IR cells in each subnucleus at each of 5 RC levels, for either sucrose (top) or QHCl (bottom; water not shown). C. FG-Fos DL cells, expressed as a percentage of FG-labeled cells in each region and on each side. D. Total FG-Fos DL cells, expressed as a percentage of Fos-IR cells. E-F: Same measurements as in C-D, except for CTb-Fos DL cells. Letters denote statistically significant groups in post-hoc tests ($p < 0.05$).